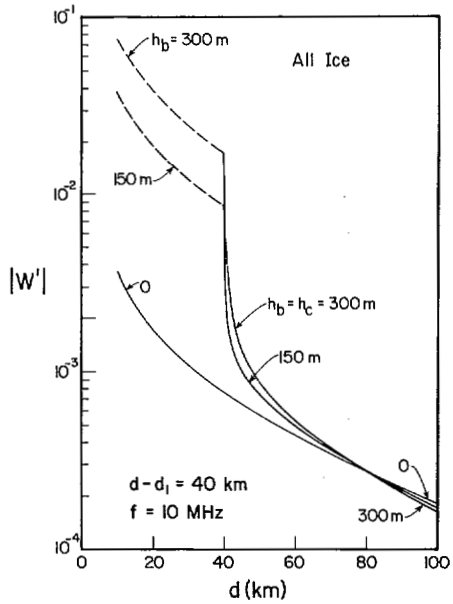

Fig. 4. Magnitude of attenuation function for an ice path. Parameters: $\epsilon/\epsilon_0 = \epsilon_1/\epsilon_0 = 6$, $\sigma = \sigma_1 = 1.67 \times 10^{-3}$ mho/m.

creases as the elevation change h_c is increased. This is consistent with the decrease in the mode conversion coefficients with increasing h_c as computed by Wait and Spies [8] for an elevation change in the earth-ionosphere waveguide.

The right section of Fig. 3 is ice with parameters $\epsilon_1/\epsilon_0 = 6$ and $\sigma_1 = 1.67 \times 10^{-3}$ mho/m, which corresponds to a loss tangent of 0.5. The electrical properties of sea ice are quite variable [10], and thin layers of low-loss sea ice can support a trapped surface wave [3]. Here we assume that the ice is sufficiently thick or lossy; it can be represented by a half space. The rapid decrease in field strength is similar to that over land in Fig. 2.

In Fig. 4 we choose an all-ice path with an elevation change to model an ice shelf. Here a large increase in field strength occurs at the elevation change because of the significant height gain of the ground wave over ice. To illustrate the height gain, $|W'|$ for $h_b = 150$ m and 300 m is also shown in the left section. For distance well beyond the elevation change, a cross-over occurs, and $|W'|$ decreases with increasing h_c.

IV. CONCLUSION

A mode-matching formulation has been utilized to compute the effect of an abrupt change in elevation on mixed-path ground-wave propagation at HF. Near the elevation change the field behavior is determined primarily by the height gain of the incident ground wave. At large distances from the boundary an elevation change results in a decrease in field strength.

Experimental data to confirm our analytical approach are not available, but a recent study by Soviet workers [11] provides a check on the mode-matching technique, where reflected waves are neglected. They consider both theory and experiment for a fin-like structure on a curved surface that is otherwise smooth. Also our results are consistent with earlier theoretical results of Furutsu [12].

REFERENCES

[1] J. R. Wait, "Recent analytical investigations of electromagnetic ground wave propagation over inhomogeneous earth models," *Proc. IEEE*, vol. 62, pp. 1061–1072, 1974.
[2] J. R. Wait and L. C. Walters, "Curves for ground wave propagation over mixed land and sea paths," *IEEE Trans. Antennas Propagat.*, vol. AP-11, pp. 38–45, 1963.
[3] D. A. Hill and J. R. Wait, "HF ground wave propagation over mixed land, sea, and sea ice paths," *IEEE Trans. Geosci. Remote Sens.*, vol. GE-19, pp. 210–216, Oct. 1981.
[4] J. R. Wait, "Diffraction and scattering of the electromagnetic groundwave by terrain features," *Radio Sci.*, vol. 3, pp. 995–1003, 1968.
[5] H. Bremmer, *Terrestrial Radio Waves*. New York: Elsevier, 1949.
[6] J. R. Wait, *Electromagnetic Waves in Stratified Media*. Oxford: Pergamon, 1962, (1970, 2nd ed.).
[7] J. C. P. Miller, *The Airy Integral*. England: Cambridge University, 1946.
[8] J. R. Wait and K. P. Spies, "VLF mode propagation across an elevated coastline," *Radio Sci.*, vol. 5, pp. 1169–1173, 1970.
[9] J. R. Wait, "On the theory of mixed-path ground-wave propagation on a spherical earth," *J. Res. Nat. Bur. Stand.*, vol. 65D, pp. 401–410, 1961.
[10] F. L. Wentworth and M. Cohn, "Electrical properties of sea ice at 0.1 to 30 Mc/s," *J. Res. Nat. Bur. Stand.*, vol. 68D, pp. 681–691, 1964.
[11] Yu. L. Lomukhin and N. B. Chimitdorzhiyev, "Increasing the decoupling between antennas arranged on a convex object," *Radio Eng. and Elect. Phys. (USSR)*, vol. 24, pp. 32–37, 1979.
[12] F. Furutsu, "Calculated curves for groundwave propagation over inhomogeneous earth with pronounced topographic features," *J. Res. Nat. Bur. Stand.*, vol. 69D, pp. 1011–1025, 1965.

A Statistical Raindrop Canting Angle Model

JOHN HOWARD, MEMBER, IEEE, AND MARIOS GEROGIOKAS

***Abstract*—A mathematical model to predict accurately the mean and standard deviation of each drop-size canting angle, assuming Gaussian canting angle distributions, is presented. The model utilizes the one-dimensional energy spectrum of horizontal turbulence given by Davenport. By using the differential equation for the horizontal-drop movement, the mean and standard deviation of each drop-size canting angle are calculated. Comparison with Saunders's work shows good agreement.**

I. INTRODUCTION

Attempts have been made by several workers (e.g., [2]–[4]) to devise a statistical canting angle model. Variations in raindrop canting angles are responsible for the variations occurring in crosspolarization discrimination measurements. All the workers to date have used the "constant canting angle" model [5], which provides an "effective mean canting angle" [6], and they have assumed a Gaussian distribution about this

Manuscript received January 24, 1980; revised June 6, 1980 and October 27, 1980.

J. Howard is with R.A.M.S. Microwave Department, Marconi Space and Defense Systems, Frimley, Chobham Road, Surrey, England.
M. Gerogiokas is with the Department of Electronics, Chelsea College, University of London, Pulton Place, London, SW6 5PR England.

0018-926X/82/0100-0141$00.75

mean with a variance calculated from their measured cross-polarization discrimination values. Recently, Howard and Mathews [7] have shown how to implement the well-known "Brussaard canting angle" model [8] to predict mean cross-polarization discrimination values for a satellite link.

In this communication, by making use of the one-dimensional energy spectrum of horizontal turbulence given by Davenport, a mathematical model estimating the mean and standard deviation of each drop size has been developed both for ground-to-ground and ground-to-satellite paths.

A. Canting Angle Variation as a Function of Wind Velocity

The differential equation for the horizontal-drop movement is given by

$$\frac{dV(t)}{dt} + \frac{g}{V_v} V(t) = \frac{g}{V_v} u(t), \tag{1}$$

where

$V(t)$ horizontal-drop velocity
V_v vertical-drop velocity (assumed to be constant and equal to the terminal velocity in stagnant air)
$U(t)$ wind velocity at the position of the drop
g gravitational constant.

Equation (1) is a linear differential equation of the first order and its solution for the mean horizontal wind velocity was given in [7]. It is repeated here in Appendix A.

In addition to the mean horizontal wind velocity there is a wind variation that can be described by

$$u = \hat{u} \cos \omega t$$

$$= \frac{\hat{\mu}}{2}(e^{j\omega t} + e^{-j\omega t}), \tag{2}$$

where

U peak horizontal-wind variation for a frequency f given by

$$\hat{u} = \sqrt{2s(f)}. \tag{3}$$

$S(f)$ energy spectrum of turbulence.

Similarly, the horizontal raindrop velocity variation can be described by

$$V = V \cos(\omega t + \varphi)$$

$$= \frac{\hat{V}}{2}(e^{j(\omega t+\varphi)} + e^{-j(\omega t+\varphi)}), \tag{4}$$

where

$\hat{V}$ peak horizontal raindrop variation for a frequency f
φ phase delay related to the response of the raindrop to wind fluctuations at a frequency f.

Using (3) and (4) in (1) we have

$$\frac{\hat{V}}{2}\left(\frac{g}{V_v} + j\omega\right) e^{j(\omega t+\varphi)} = \frac{\hat{u}}{2}\frac{g}{V_v} e^{j\omega t} \tag{5a}$$

$$\frac{\hat{V}}{2}\left(\frac{g}{V_v} - j\omega\right) e^{-j(\omega+\varphi)} = \frac{\hat{u}}{2}\frac{g}{V_v} e^{-j\omega t} \tag{5b}$$

$$\hat{V}\cos(\omega t + \varphi) = \frac{\hat{u}}{2}\left(\frac{g/V_v}{g/V_v + j\omega} e^{j\omega t} + \frac{g/V_v}{g/V_v - j\omega} e^{-j\omega t}\right). \tag{6}$$

It is known [8] that

$$\tan \vartheta_v = \frac{u - V}{V_v}, \tag{7}$$

where

ϑ_v canting angle of a raindrop due to the wind variations.

Then,

$$\tan \vartheta_v = \left(\frac{\hat{u}\cos \omega t - \hat{V}\cos(\omega t + \varphi)}{V_v}\right)$$

$$= \frac{\hat{u}}{2V_v}\left(\left(1 - \frac{g/V_v}{g/V_v + j\omega}\right) e^{j\omega t} + \left(1 - \frac{g/V_v}{g/V_v - j\omega}\right) e^{-j\omega t}\right)$$

$$= \frac{\hat{u}}{V_v}\frac{1}{\sqrt{1 + (g/V_\omega V_v)^2}} \cdot \frac{e^{j(\omega t + \tan^{-1} g/\omega V_v)} + e^{-j(\omega t + \tan^{-1} g/\omega V_v)}}{2} \tag{8}$$

$$\tan \vartheta_v = \frac{\hat{u}}{V_v}\frac{1}{\sqrt{1 + (g/\omega V_v)^2}} \cos(\omega t + \tan^{-1} g/\omega V_v). \tag{9}$$

The total canting angle can be obtained from

$$\tan \vartheta = \tan \vartheta_0 + \tan \vartheta_v, \tag{10}$$

where

ϑ_0 mean canting of a raindrop (see (A13) or (A15)).

From (10) we have

$$\vartheta = \vartheta_0 + \tan^{-1}\left(\frac{\tan \vartheta_v}{1 + \tan^2 \vartheta_0 + \tan \vartheta_0 \tan \vartheta_v}\right). \tag{11}$$

From a study of about 70 spectra of turbulence, Davenport suggested the following empirical expression for the energy spectrum of turbulence:

$$S(f) = \frac{4.0\, C_D u_1^2}{f}\frac{x^2}{(1 + x^2)^{4/3}}, \tag{12}$$

where

$S(f)$ energy spectrum of turbulence, invariant with height

f frequency of wind variation

U_1 velocity at a reference height near the ground (usually at the standard reference height of 10 m)

C_D drag coefficient given by [10]

$$C_D = \left(\frac{k}{\ln \frac{10}{20}} \right)^2$$

Z_0 constant depending on the terrain compared with the reference height of 10 m, and k is Von Karman's constant ($k \approx 0.4$) and

$$x = \frac{1200\, f}{u_1}.$$

Using (11) and (12) the standard deviation of the canting angle of a single raindrop size can be computed from

$$\sigma_\vartheta = \left[\int_0^\infty \left(\tan^{-1} \left(\frac{\tan \vartheta_v}{1 + \tan^2 \vartheta_0 + \tan \vartheta_0 \tan \vartheta_v} \right) \right)^2 \cdot S(fi)\, df \right]^{1/2}. \quad (13)$$

In a paper by Saunders [2] the distribution of canting angles during two rainstorms is given, using the images of 463 raindrops obtained with a raindrop camera [11], [12] by personnel at the Illinois State Water Survey.

In order to compare Saunders's results with the mathematical model presented in this communication, further information was needed in addition to the mean horizontal wind speed of 15 m/s and the precipitation rate of 28 mm/h provided; namely, 1) the height of the raindrop camera, and 2) the type of the terrain where the measurements were taken. The information supplied to the authors [13], [14] indicated that 1) the height of the camera was between 3–5 ft, (the authors assumed a height of 1.5 m, though strictly speaking, all equations in this communication apply at heights greater than 10 m), and 2) the type of the terrain was assumed to be "a flat countryside with some form of short vegetation." The authors therefore assumed z_0 as having the value of 0.10 m.

Assuming the above and using (A15) with $m \approx 0.2$ in Appendix A and (13) the mean and standard deviation of the canting angle of each raindrop size were calculated. These are provided in Table I, whereas Table II shows the same calculations for a mean horizontal wind velocity of 10 m/s.

Assuming a Gaussian canting angle distribution for each drop size and weighting each drop-size distribution according to the number of drops for each size, we have plotted the fraction of raindrop population with canting angles $\geqslant \vartheta$ and $\leqslant -\vartheta$ degrees, as in Saunders's Fig. 2. This is shown in Fig. 1 compared with Saunders's graph for the 28 mm/hr precipitation rate and 15 m/s mean wind velocity.

In Fig. 2 the fraction of raindrop population, with canting angles $\geqslant \vartheta$ and $\leqslant -\vartheta$ degrees for 25 mm/h precipitation rate and horizontal-wind velocities of 15 m/s and 10 m/s, is shown. Fig. 3 shows the fraction of total drops having canting angles in a 10° interval for 25 mm/h precipitation rates and horizontal wind velocities of 15 m/s and 10 m/s.

TABLE I
MEAN AND STANDARD DEVIATION OF CANTING ANGLE[1]

Drop Radius (meters)	(Degrees)	(Degrees)
0.00025	13.5	41.8
0.00050	19.6	34.9
0.00075	21.7	32.7
0.00100	22.6	31.6
0.00125	23.1	31.0
0.00150	23.4	30.7
0.00175	23.5	30.5
0.00200	23.6	30.3
0.00225	23.6	30.3
0.00250	23.6	30.3
0.00275	23.6	30.2
0.00300	23.6	30.2
0.00325	23.6	30.2

[1] Mean horizontal wind velocity $U_1 = 15$ m/s, measured at height $h_r = 10$ m, height of observations $h = 1.5$ m, drag coefficient $C_D \approx 0.008$, $m \approx 0.2$.

TABLE II
MEAN AND STANDARD DEVIATION OF CANTING ANGLE[2]

Drop Radius (meters)	(Degrees)	(Degrees)
0.00025	9.2	18.0
0.00050	13.4	16.1
0.00075	14.9	15.4
0.00100	15.6	14.9
0.00125	16.0	14.8
0.00150	16.1	14.6
0.00175	16.2	14.5
0.00200	16.3	14.5
0.00225	16.3	14.4
0.00250	16.3	14.4
0.00275	16.3	14.4
0.00300	16.3	14.4
0.00325	16.3	14.4

[2] Mean horizontal wind velocity $U_1 = 10$ m/s, measured at height $h_r = 10$ m, height of observations $h = 1.5$ m, drag coefficient $C_D \approx 0.008$, $m \approx 0.2$.

DISCUSSION AND CONCLUSION

In this communication we are interested in calculating an estimate of the mean and standard deviation of the canting angle for the individual raindrop sizes. This is used for the calculation of the crosspolarization discrimination values in both ground and satellite microwave links.

In order to use the model one needs to have a knowledge of a) the precipitation rate, b) the mean horizontal wind speed at a reference height, and c) the type of terrain.

It is to be noted that near neutral atmospheric conditions are assumed—a situation most likely to exist when it is raining [15].

Compared with Saunders's measured canting angle distributions the model shows good agreement. The difference between Saunders's results and our results in Fig. 1 are probably due to a) inaccuracies introduced by the raindrop camera, used by Saunders, in producing the images of small drops, b)

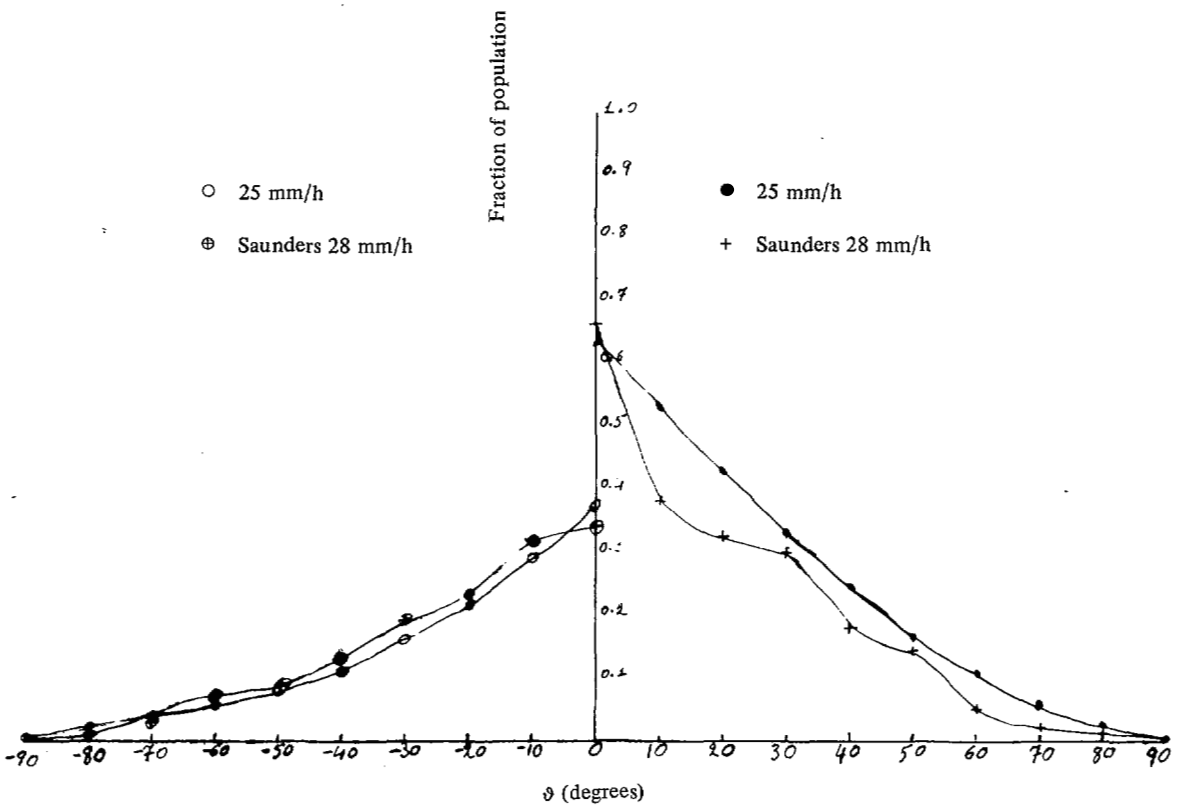

Fig. 1. Fraction of raindrop population with canting angles $\geq \vartheta$ and $\leq -\vartheta$. $U_1 = U_0 = 15$ m/s, $h = 1.5$ m (comparison with Saunders).

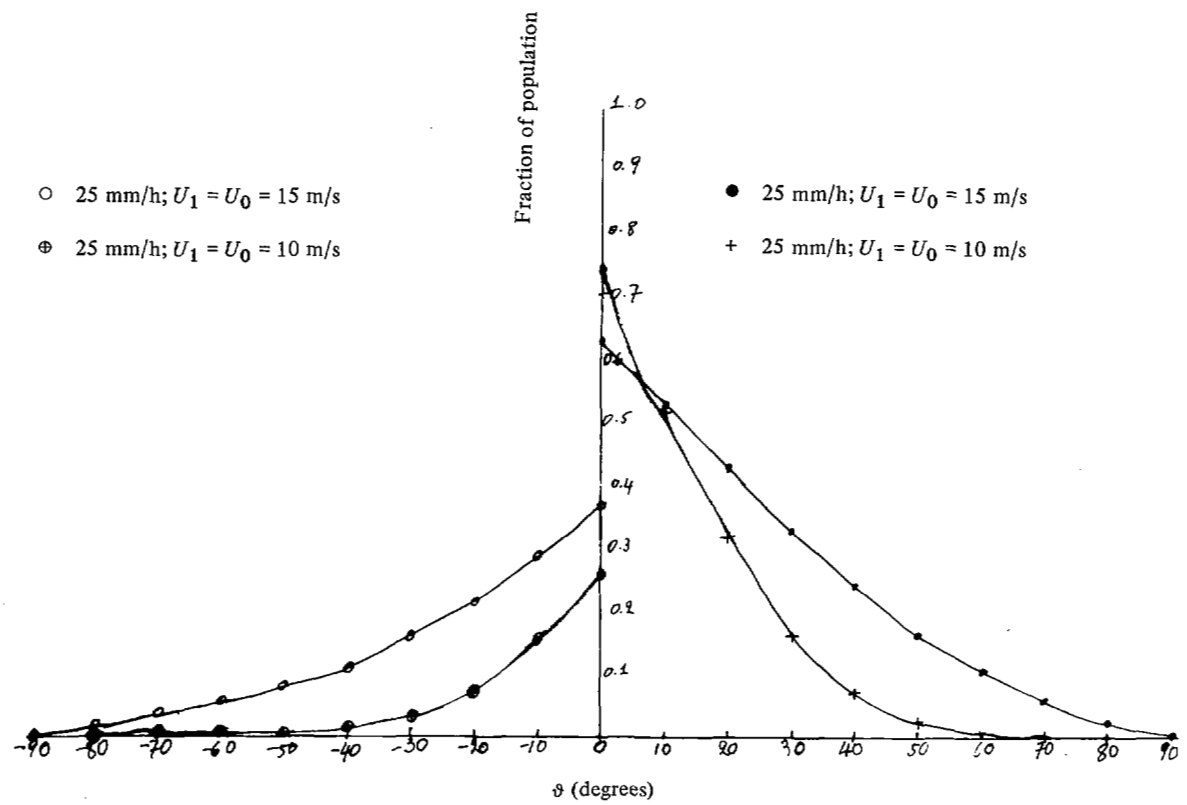

Fig. 2. Fraction of raindrop population with canting angles $\geq \vartheta$ and $\leq -\vartheta$, $h = 1.5$ m.

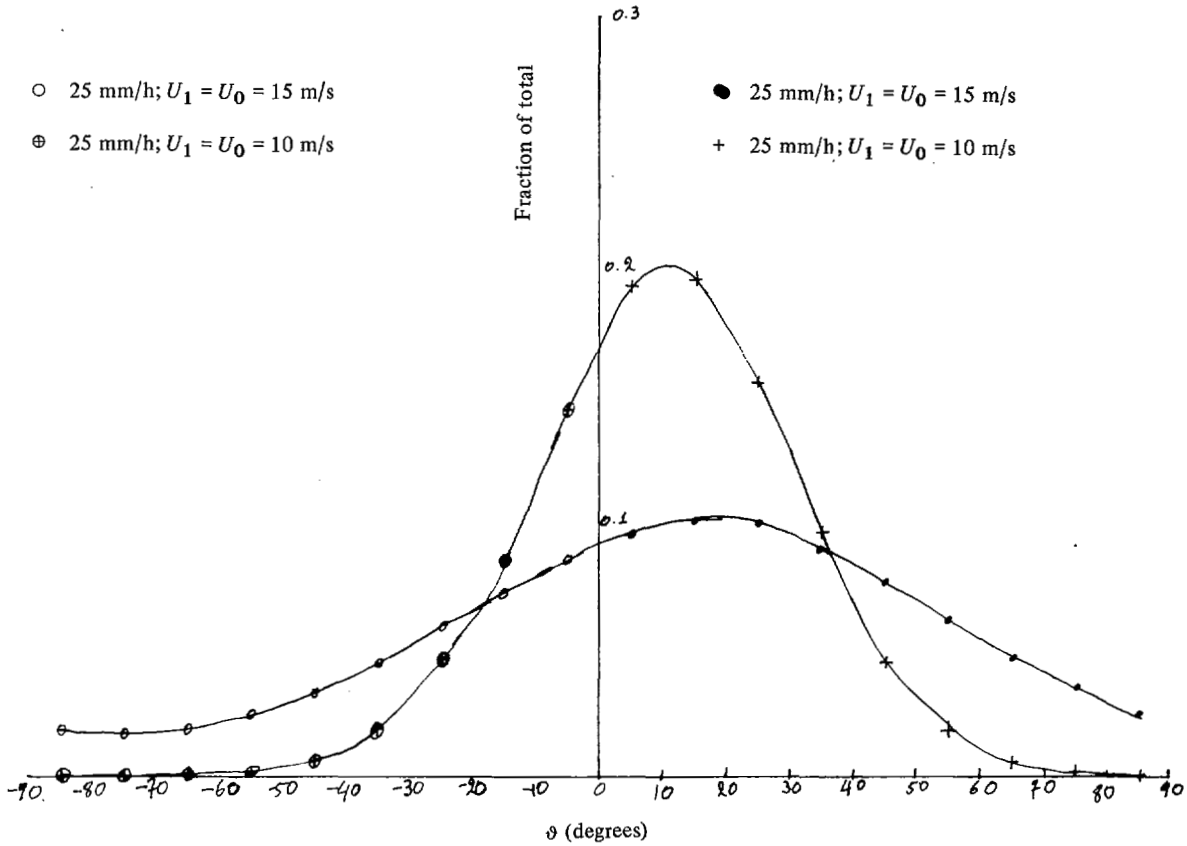

Fig. 3. Fraction of total drops (1356) having canting angles in 10° interval, $h = 1.5$ m.

the sample of 259 drops that Saunders used to calculate its canting angle distribution being too small for an accurate canting angle distribution to be drawn, and c) the equations used in this communication applicable at heights equal to or greater than 10 m, not completely describing horizontal wind velocity variations and generally effects of atmospheric conditions on canting angles in a precipitation environment.

From Fig. 2 it can be seen that the higher the mean horizontal wind velocity the larger the spread of the canting angles. This can also be concluded from (12).

Fig. 3 shows the fraction of total drops having canting angles in a 10° interval. This graph can be used to evaluate the mean and variance of the effective canting angle for the constant canting angle model, although it will be more accurate to evaluate them from Tables I and II. It must be noted that in the former case the ordinate values must be divided by the ϑ interval (in radian). As an example, in the case of the 15 m/s mean horizontal wind velocity we obtain a mean canting angle of 15.9° and a standard deviation of 39°.

APPENDIX A

CALCULATION OF THE MEAN CANTING ANGLE ϑ_0

The differential equation for the horizontal drop movement is given by

$$\frac{dV(t)}{dt} + \frac{g}{V_v} V(t) = \frac{g}{V_v} u(t) = 0, \tag{A1}$$

where

V horizontal drop velocity
U wind velocity at the position of the drop
V_v vertical drop velocity (assumed to be constant and equal to the terminal velocity in stagnant air)
g gravitational constant.

Equation (A1) is a linear differential equation of the first order and therefore has the following general solution:

$$V(t) = Ce^{-(g/V_v)t} + g/V_v e^{-(g/V_v)t} \int_0^t u(t) e^{(g/V_v)t}\, dt. \tag{A2}$$

Assuming that there is no updraught the height of the drop follows from

$$h(t) = h(0) - V_v t. \tag{A3}$$

Using (A3) in (A1) we have

$$\frac{dV(h)}{dh} - \frac{g}{V_v{}^2} V(h) + \frac{g}{V_v{}^2} u(h) = 0. \tag{A4}$$

The solution of (A4) is given by

$$V(h) = C_1 e^{(g/V_v{}^2)h} - g/V_v{}^2 e^{(g/V_v{}^2)h} \cdot \int_0^h e^{-(g/V_v{}^2)y} u(y)\, dy \tag{A5}$$

$$C_1 = \lim_{h\to\infty} \left(V(h)e^{-(g/V_v{}^2)h} + g/V_v{}^2 \int_0^h e^{-(g/V_v{}^2)y} u(y)\,dy \right)$$

$$= 0 + g/V_v{}^2 \int_0^\infty e^{-(g/V_v{}^2)y} u(y)\,dy. \tag{A6}$$

Using (A6) in (A5) we get

$$V(h) = g/V_v{}^2 e^{(g/V_v{}^2)h} \left(\int_0^\infty e^{-(g/V_v{}^2)y} u(y)\,dy - \int_0^h e^{-(g/V_v{}^2)y} u(y)\,dy \right)$$

$$= g/V_v{}^2 e^{(g/V_v{}^2)h} \int_h^\infty e^{-(g/V_v{}^2)h} u(y)\,dy. \tag{A7}$$

For neutral conditions the mean horizontal wind velocity varies with height in a logorithmic manner [10] as

$$u(y) = \frac{u^*}{K} \ln\left(\frac{y}{Z_0}\right), \tag{A8}$$

where,

- u^* friction velocity
- K Karman's constant
- Z_0 constant depending on the terrain.

Therefore,

$$V(h) = u(h) + \frac{u^*}{K} e^{(g/V_v{}^2)h} \int_h^\infty \frac{e^{-(g/V_v{}^2)y}}{y}\,dy \tag{A9}$$

or

$$V(h) = U(h) + \frac{u^*}{K} e^{(g/V_v{}^2)h} \cdot \int_{(g/V_v{}^2)h}^\infty \frac{e^{-(g/V_v{}^2)y}}{(g/V_v{}^2)y}\,d(g/V_v{}^2)y. \tag{A10}$$

But [16]

$$\int_2^\infty \frac{e^{-t}}{t}\,dt = E_1(z), \tag{A11}$$

where

$E_1(z)$ the exponential integral.

Using (A11) in (A10) we obtain

$$V(h) = u(h) + \frac{u^*}{K} e^{(g/V_v{}^2)h} E_1(g/V_v{}^2 h). \tag{A12}$$

The mean canting angle for each raindrop can be obtained from

$$\tan\vartheta_0 = \frac{u(h) - V(h)}{V_v} = \frac{u^*}{K} e^{(g/V_v{}^2)h} E_1(g/V_v{}^2 h). \tag{A13}$$

The dependence of the wind velocity on height may be also described by a power law for heights up to 300 m,

$$\frac{u(h)}{u_r} = \left(\frac{h}{h_r}\right)^m \tag{A14}$$

where

- U_r wind velocity measured at a reference height h_r (e.g., 10 m)
- m a constant dependent on the roughness of the terrain ranging from 0.1 for sea to 0.3–0.4 for large cities.

Using (A14) in (A7) the mean canting angle for each raindrop can be obtained from [8]

$$\tan\vartheta_0 = \frac{V_0}{g} u' x^{1-m} e^x \Gamma(m, x), \tag{A15}$$

where

$$u' = \frac{du}{dh}$$

$$x = \vartheta/V_v{}^2 h.$$

$$\Gamma(m, x) = \int_2^\infty e^{-p} p^{m-1}\,dp. \tag{A15}$$

Equations (A13) and (A15) should be applied at heights greater than 10 m. For heights lower than 10 m (A15) seems to give more realistic results.

ACKNOWLEDGMENT

The authors wish to thank M. J. Saunders of Bell Telephone Laboratories, GA; D. M. A. Jones of the Illinois State Water Survey, Urbana; F. B. Smith of the Meterological Office, Bracknell, England; J. Dyster, colleague at Marconi Space and Defence Systems Ltd., Frimely, England, for many stimulating and helpful discussions.

REFERENCES

[1] A. G. Davenport, "The spectrum of horizontal gustiness near the ground in high winds," *Quart. J.R. Met. Soc.*, vol. 87, no. 2, pp. 194–211, Apr. 1961.

[2] M. J. Saunders, "Crosspolarization at 18 and 30 GHz due to rain," *IEEE Trans. Antennas Propat.*, vol. AP-19, no. 2, pp. 273–277, Mar. 1971.

[3] W. L. Nowland, R. L. Olsen, and L. P. Shkarofsky, "Theoretical relationship between rain depolarization and attenuation," *Electron. Lett.*, vol. 13, no. 22, pp. 676–678, Oct. 1977.

[4] I. J. Dilworth and B. G. Evans, "Preliminary results of linear/circular depolarization on 18 Km, 11.6 GHz radio link," *Electron. Lett.*, vol. 12, no. 23, pp 618–620, Nov. 1976.

[5] P. A. Watson, "Crosspolarization measurements at 11 GHz," *Proc. Inst. Elec. Eng.*, vol. 123, no. 7, pp. 667–675, July 1976.

[6] I. J. Dilworth and B. G. Evans, "Cumulative crosspolarization and canting angle distributions," *Electron. Lett.*, vol. 15, no. 19, pp. 603–604, Sept. 1979.

[7] J. Howard and N. A. Mathews, "Crosspolarization of microwaves due to rain on a satellite to earth path," *IEEE Trans. Antennas Propagat.*, vol. AP-27, no. 6, pp 890–891, Nov. 1979.
[8] G. Brussaard, "A meteorological model for rain-induced cross-polarization," *IEEE Trans. Antennas Propagat.*, vol. AP-24, no. 1, pp 5–11, Jan. 1976.
[9] B. O. Mahen and P. J. Murphy, "Variation of canting-angle distribution as a function of wind velocity," *Electron. Lett.*, vol. 13, no. 19, pp 567–568, Sept. 1977.
[10] F. B. Smith, "Turbulence in the atmospheric boundary layer," *Sci. Prog.*, Oxford, vol. 62, pp 127–151, 1975.
[11] D. M. A. Jones and L. A. Dean, "A raindrop camera," U.S. Army Signal Corps Engineering Laboratories, Fort Monmouth, NJ, Res. Rep. 3, Contract DA-36-039 SC-42446, Dec. 1953.
[12] D. M.A. Jones, "The shape of raindrops," *J. Meteorol*, vol. 16, no. 6, pp. 504–510, Oct. 1959.
[13] M. J. Saunders, personal communication.
[14] D. M. A. Jones, personal communication.
[15] F. B. Smith, personal communication.
[16] M. Abramowitz and I. A. Stegun, *Handbook of Mathematical Functions*. New York: Dover, 1972.
[17] R. A. Semplak, "Measurements of rain—induced polarization rotation at 30.9 GHz," *Radio Sci.*, vol. 9, no. 4, pp 425–429, Apr. 1974.

Radiation from Flanged Waveguide: Comparison of Solutions

SHUNG-WU LEE AND LEON GRUN

Abstract—**The reflection coefficient of the transverse electric (TE_1) mode in a flanged parallel-plate waveguide is considered, its solutions derived by the four different methods are numerically compared.**

Consider the radiation from a flanged parallel-plate waveguide as is sketched in Fig. 1. This fundamental problem is exactly solvable only for the special case $m = 2$, where $m\pi$ is the exterior angle of the wedges forming the guide. For an arbitrary value of m, solutions available are those calculated by ray techniques [1], [2], published more than ten years ago. It is well-known that ray solutions are asymptotic in nature and that their accuracy is generally difficult to assess. In a recent article MacPhie and Zaghloul [3] gave "an exact (numerical) solution by the correlation matrix method" for the flanged parallel-plate waveguide with $m = 3/2$. It is therefore useful to compare numerically the ray solutions with the MZ solution.

For the incident transverse electric (TE_n) mode with n odd (symmetrical mode), the reflection coefficient Γ_n calculated by the ray method described in [2] is (for $\exp(-i\omega t)$ time convention)

$$\Gamma_n = \left\{ \frac{-i}{2ka\cos\phi_n} \right\} (\chi^i - \chi^r)[G_+(k\cos\phi_n)]^2, \qquad n = 1, 3, 5, \cdots. \tag{1}$$

Manuscript received November 22, 1980; revised June 11, 1981. This work was supported by the Air Force Office of Scientific Research under Grant AFOSR 80-0179.

The authors are with the Electromagnetics Laboratory, Department of Electrical Engineering, University of Illinois, Urbana, IL 61801.

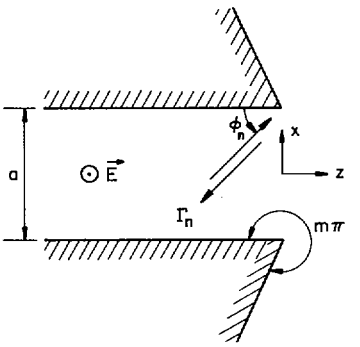

Fig. 1. Radiation from flanged parallel-plate waveguide. Γ_n is self-reflection coefficient of TE_n mode.

Here the factor in braces is the ray-to-mode conversion factor and the modal angle of the TE_n mode is

$$\phi_n = \sin^{-1}(n\lambda/2a), \qquad n = 1, 3, 5, \cdots. \tag{2}$$

Wedge diffraction coefficients $\chi^{i,r}$ are defined in [4, eq. (4.10)] and are given by

$$\chi^{i,r} = \frac{\frac{2}{m}\sin\frac{\pi}{m}}{\cos\frac{\pi}{m} - \cos\frac{\phi_n \mp \phi_n}{m}}. \tag{3}$$

The factorization function G_+ is given in [2, eq. (6.11)] ($a = 2b$ and is tabulated in [10]. Two remarks about (1) are in order. a) This solution is a generalization of [2, eq. (7.3c)] which applies only for the special case $m = 2$ (no flange). For $m = 2$, (1) agrees with the exact solution obtainable by the Wiener–Hopf technique. b) For an incident transverse electromagnetic (TEM) mode and with $m = 3/2$ a corresponding ray solution of (1) checks very well with that obtained by a generalized mode-matching procedure [5]. For the radiation problem in Fig. 1, the YFK solution [1] is the same as (1) except that the definition of G_+ is different.

For $n = 1$ and $m = 3/2$ we calculate Γ_1 from (1) as a function of a/λ. Some results are presented in Table I and Fig. 2, where we also plot the YFK results taken from [1, Figs. 8d and 8e]. Note that these two ray solutions are generally in excellent agreement, except that near $a = 1.5\lambda$ (onset of TE_3 mode) the YFK solution fails to give the discontinuous derivatives in the curves. (This is best seen from the original figures in [1].) It is worthwhile to mention that an improvement of the YFK solution using a more elaborate ray method (the uniform asymptotic theory of diffraction) is given by Boersma [6]. Two other methods for calculating Γ_1 are given in [8][1] and [9]. For $a > 0.8\lambda$ their numerical results are in good agreement with that of YFK, and therefore with the present ray solution in (1).

We now compare the ray solution in (1) with the MZ solution [3, Fig. 4] and Marcuvitz solution [7, p. 192]. The nor-

[1] Because of the difference in definition and time convention, Z/Z_0 used here is equal to $(a/240\pi)(G_a - iB_a)^{-1}$ in [8].

0018-926X/82/0100-0147$00.75